Analytical description of the dispersion relation for phase resonances in compound transmission gratings

Isroel M. Mandel
Department of Physics, Graduate Center, City College of the City University of New York, New York, New York 10031, USA

Andrii B. Golovin
Department of Electrical Engineering, Center for Metamaterials, City College of the City University of New York, New York, New York 10031, USA

David T. Crouse*
Department of Electrical Engineering, Center for Metamaterials, The City College of New York, New York, New York 10031, USA
(Received 26 July 2012; revised manuscript received 28 September 2012; published 24 May 2013)

An analytical approach is used to describe the dispersion of phase resonances occurring between waveguide cavity modes in compound transmission gratings. The strongly enhanced evanescent fields associated with the phase resonances are used to derive an approximate closed-form equation for the dispersion of phase resonances. The equation that is derived predicts the dependence of the frequencies and dispersion of the phase resonances on structural feature sizes, material parameters, and the momentum of the phase resonance. This analytical description is compared to results obtained by using a rigorous coupled wave algorithm. This equation allows one to design a compound transmission grating that supports phase resonances with particular properties, such as resonant frequencies and momenta. Applications of the phase resonances to high-finesse electromagnetic filters and corrugated surface antennas are discussed.

DOI: 10.1103/PhysRevA.87.053833 PACS number(s): 42.25.Fx, 41.20.Jb, 42.79.−e

I. INTRODUCTION

Patterned materials have been shown to produce anomalous optical effects, including extraordinary optical transmission in periodically perforated metal films (produced either by surface plasmons [1–5] or by waveguide cavity modes [6–8]), high electromagnetic- (EM-) field enhancements near patterned metal surfaces (i.e., plasmonic structures) [9], and unusual light channeling properties of transformational optical materials [10–12]. Included within this list of extraordinary optical phenomena and structures should be phase resonances (PRs) and the structures that support them. PRs are coupled cavity modes within cavities in one-dimensionally periodic compound reflection gratings (CRGs) [13,14], compound transmission gratings (CTGs) [8,15–19], or in two-dimensionally (2D) periodic cavity and hole arrays. Whereas, simple lamellar gratings (SLGs) have only one groove in the infinitely repeated unit cell, CRGs and CTGs have multiple grooves within the unit cell with these multiple grooves having some difference or dissimilarity between them (Fig. 1). These differences can be different widths, dielectric filling materials, different distances to neighboring grooves on their left-hand sides (LHSs) and right-hand sides (RHSs), or some other aspect that makes them not identical with respect to each other. For incident light of particular frequencies and angles of incidence, these structures can support PRs in which waveguide cavity modes (WCMs) within the multiple grooves in the unit cell couple strongly with each other as energy is transferred back and forth between the cavities. This coupling results in an extraordinary buildup of energy as the incident beam of light is captured by the PR. For some types of CTGs composed of lossless materials, this buildup of energy and light concentration is comparable to, or higher than, what is achievable with surface plasmons, photonic crystals, and other optical modes [20].

PRs have been numerically modeled and experimentally measured in numerous CRGs and CTGs [8,13,15–19,21,22]. However, there have been far fewer papers on theoretical and analytical models of PRs that would provide valuable information on the EM-field profiles, the frequency and bandwidth of the resonances, the dispersion of the modes, the phase and group velocities, and the EM-field enhancements of the modes [21–23]. But there are two papers of merit on analytical models of PRs. One paper is by Medina and Mesa on a circuit model of extraordinary transmission and PRs that predicts the optical properties of PRs once values for capacitance parameters are determined by a 2D Laplace equation solver [22]. Complementary to the circuit model is the analytic model using a modal method, developed for particular CTGs in Refs. [21,23] and further developed in this paper for particular structures. In the papers by Fantino *et al*. [21] and Skigin [23], a modal method is used in a very similar way as used in the first part of this paper, yet they focus on CRGs with many grooves in the unit cell (up to 19 in the case of Ref. [21] and an arbitrary number in Ref. [23]) and show how to use a modal method to numerically determine the EM fields that compose PRs, the frequency at which PRs occur, and the reflectance of the structure. In Ref. [23], the frequencies of PRs in CTGs are approximately determined numerically by solving for the frequencies at which particular functions go to zero. At such frequencies, the amplitudes of the WCMs in the grooves become large relative to the excitation beam (by factors exceeding 10^6), this being one of the salient properties of PRs.

*dcrouse@ccny.cuny.edu

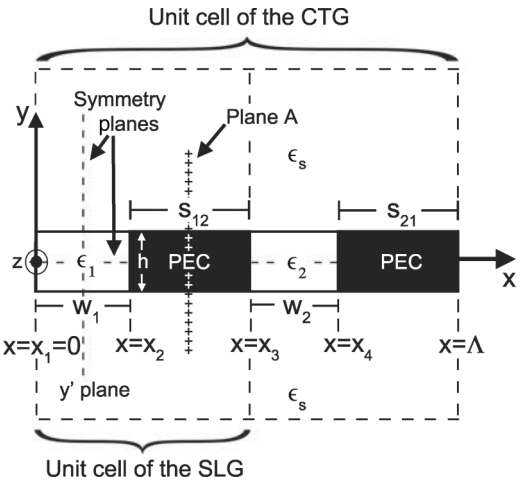

FIG. 1. The 2-groove CTG studied in this paper. The metal is considered as a perfect electrical conductor (PEC). If the grooves are identical and if $s_{12} = s_{21}$, then the CTG converts to a SLG with a period of $x_3 = \Lambda/2$. There are two planes of mirror symmetry in the physical structure, namely, the x-z and y-z planes. Mirror symmetry about Plane A needs to be broken in order for the CTG to support PRs.

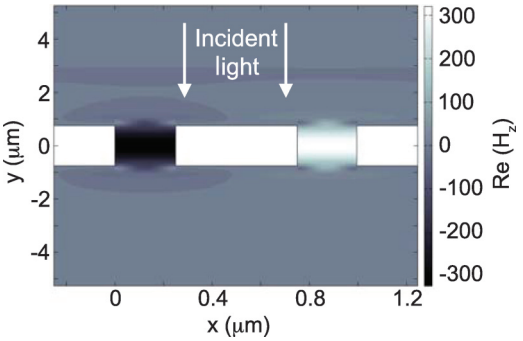

FIG. 2. (Color online) The PR supported by the 2-groove CTG studied in this paper. The CTG has a thickness of $h = 1.5$ μm and a period of $\Lambda = 1.45$ μm with the unit cell that includes the two dissimilar vacuum-filled grooves through a PEC metal film; the left groove has a width of $w_1 = 0.25$ μm, and the right groove has a width of $w_2 = 0.245$ μm; the substrate and superstrate are vacuums. The magnetic field Re(H_z) of the PR excited by 0.337 eV ($\lambda = 3.681$ μm) normal incident TM polarized light of unit amplitude ($I_0 = 1$) is shown. It is seen that this PR has a highly enhanced field with field amplitudes over 300 times greater than the incident beam that excites the PR (yielding an *intensity* enhancement and Q of over 10^4). The figure also shows that the enhanced fields in the two grooves have π-rad relative phase differences.

The main focus of this paper is the use of an analytic method to study the properties of PRs and to calculate a closed-form expression for the frequencies and momenta of the PRs (i.e., the dispersion relation) that occur as a structure undergoes a *transition* from a SLG to a CTG as one introduces an *infinitesimally small* difference in the geometry or composition of *every other* groove in the structure. This perturbation in the structure results in the breaking of a symmetry of the system that enables the structure to support PRs. Thus, the CTG studied in this paper will have two only slightly dissimilar grooves within the unit cell, referred to as a 2-groove CTG. It is at this SLG → CTG transition where the PRs have the most compelling properties, i.e., extraordinarily narrow bandwidths and large field intensities relative to the incident beams that excite them (see Fig. 2). The existence of a simple closed-form equation that predicts the frequencies of PRs (ω_{pr}) would be very useful because the PRs in low-loss or lossless structures can have such narrow bandwidths that resolving them with the finite-element method (FEM) and finite-difference time-domain (FDTD) algorithms can be difficult [23]. This equation can then be used to design a CTG with PRs with desired properties, frequencies, and momenta. The equation can also be used to determine the frequency around which frequency sweeps using FEM and FDTD models should be performed to capture the optical effects of PRs. In this paper, all the details of the mathematics of the analytical model and rigorous coupled wave algorithm (RCWA) have been shown so as to allow the reader to implement these methods, however, these lengthy calculations reduce down to a simple closed-form expression from which one can extract the frequencies (ω_{pr}) and momenta (k_x) of PRs,

$$\frac{2i\gamma_0}{\epsilon_g}\tan\left(\gamma_0\frac{h}{2}\right) = \frac{\beta_1\beta_{-1}(\Lambda/\epsilon_s w)}{\beta_1\mathrm{sinc}^2\left(\alpha_{-1}\frac{w}{2}\right)+\beta_{-1}\mathrm{sinc}^2\left(\alpha_1\frac{w}{2}\right)}, \tag{1}$$

with $\beta_{\pm1} = (\epsilon_s k_o^2 - \alpha_{\pm1}^2)^{1/2}$, $\alpha_{\pm1} = k_x \pm K$, $\gamma_0 = \sqrt{\epsilon_g}k_o$, and $k_o = \omega_{pr}/c$, where $K = 2\pi/\Lambda$, Λ is the period of the 2-groove CTG (i.e., the length of the unit cell that contains *both* grooves), ϵ_s is the dielectric constant of the superstrate and substrate (both are composed of the same material), h is the height of the grooves, w and ϵ_g are the widths and dielectric constants, respectively, of both grooves before the perturbation is introduced in either of these two values, and the sinc function is $\mathrm{sinc}(x) = \sin(x)/x$. The solutions of Eq. (1) for ω_{pr} for a range of k_x values can be obtained to yield the full dispersion curve of PRs in 2-groove CTGs.

This paper is organized as follows: First, a RCWA is summarized. Second, the resulting set of equations is simplified to obtain the relation describing the dispersion relation of PRs [i.e., Eq. (1)]. Third, the results predicted by this relation are compared with results obtained from a full RCWA algorithm.

II. RIGOROUS COUPLED WAVE ALGORITHM

The RCWA in this paper has been described in several prior papers [6,21,23] and has been used to model periodically patterned metal-dielectric structures with and without optical loss in the materials. Important aspects of the RCWA algorithm will be described in this paper because numerous aspects of the calculation and the EM-field expansion modes will be discussed throughout the remainder of this paper; a more thorough description of the RCWA can be found in Ref. [6]. For structures with optical loss, a surface impedance boundary condition can be used to include loss and to describe the field penetration into the metals [6]. For structures without loss, the metals are treated as PECs. In either case of lossless or lossy structures, the RCWA algorithm expresses the fields in the semi-infinite homogeneous superstrate (i.e., the topmost layer) and the substrate as a linear combination of Floquet modes and

expresses the fields in the two dissimilar grooves in the unit cell as linear combinations of WCMs. And because the metals are assumed to be PECs, the fields within the metal are assumed to be zero. In this RCWA algorithm, all the electromagnetic-field components have a $\exp(-i\omega t)$ time dependence, and cgs units are used throughout the calculation.

For the top superstrate, the fields for TM Floquet modes are expressed in terms of downward (upward) incident (scattered) beams with field expansion coefficients I_n^t (R_n^t); and in the bottom substrate, the TM modes are expressed in terms of upward (downward) incident (scattered) beams with field expansion coefficients I_n^b (R_n^b),

$$H_z^{(\substack{t\\b})} = \sum_{n=-\infty}^{n=\infty} I_n^{(\substack{t\\b})} \exp\left\{i\left[\alpha_n\left(x-\frac{w_1}{2}\right) \mp \beta_n\left(y-\frac{h}{2}\right)\right]\right\} + R_n^{(\substack{t\\b})} \exp\left\{i\left[\alpha_n\left(x-\frac{w_1}{2}\right) \pm \beta_n\left(y-\frac{h}{2}\right)\right]\right\}, \tag{2a}$$

$$E_x^{(\substack{t\\b})} = \frac{1}{\epsilon_s k_o} \sum_{n=-\infty}^{n=\infty} \pm\beta_n I_n^{(\substack{t\\b})} \exp\left\{i\left[\alpha_n\left(x-\frac{w_1}{2}\right) \mp \beta_n\left(y-\frac{h}{2}\right)\right]\right\} \mp \beta_n R_n^{(\substack{t\\b})} \exp\left\{i\left[\alpha_n\left(x-\frac{w_1}{2}\right) \pm \beta_n\left(y-\frac{h}{2}\right)\right]\right\}, \tag{2b}$$

$$E_y^{(\substack{t\\b})} = \frac{1}{\epsilon_s k_o} \sum_{n=-\infty}^{n=\infty} \alpha_n I_n^{(\substack{t\\b})} \exp\left\{i\left[\alpha_n\left(x-\frac{w_1}{2}\right) \mp \beta_n\left(y-\frac{h}{2}\right)\right]\right\} + \alpha_n R_n^{(\substack{t\\b})} \exp\left\{i\left[\alpha_n\left(x-\frac{w_1}{2}\right) \pm \beta_n\left(y-\frac{h}{2}\right)\right]\right\}. \tag{2c}$$

Also used in Eqs. (2) are the relations,

$$\alpha_n = k_x + nK, \tag{3}$$

$$\beta_n = \left(\epsilon_s k_o^2 - \alpha_n^2\right)^{1/2}, \tag{4}$$

with k_x as the net momentum in the $\hat{x}$ direction of the Floquet modes, $k_o = \omega/c$, with ω being the frequency of the incident light. Note that Eq. (4) applies to both the superstrate and the substrate because it is assumed that they are composed of the same material.

As for the fields in the cavities, they are expressed as a superposition of upward propagating (or upwardly evanescently decaying) waveguide cavity modes with expansion coefficients a_m^g and downward propagating (or downwardly evanescently decaying) waveguide cavity modes with expansion coefficients b_m^g with $g = 1$ for groove 1 and $g = 2$ for groove 2,

$$H_z^g = \sqrt{\frac{2}{w_g}} \sum_{m=0}^{\infty} \cos\left[\mu_m^g\left(x - x_o^g\right)\right]\left(a_m^g e^{i\gamma_m^g y} + b_m^g e^{-i\gamma_m^g y}\right), \tag{5a}$$

$$E_x^g = -\frac{1}{\epsilon_g k_o}\sqrt{\frac{2}{w_g}} \sum_{m=0}^{\infty} \gamma_m^g \cos\left[\mu_m^g\left(x - x_o^g\right)\right] \times \left(a_m^g e^{i\gamma_m^g y} - b_m^g e^{-i\gamma_m^g y}\right), \tag{5b}$$

$$E_y^g = \frac{i}{\epsilon_g k_o}\sqrt{\frac{2}{w_g}} \sum_{m=0}^{\infty} \mu_m^g \sin\left[\mu_m^g\left(x - x_o^g\right)\right] \times \left(a_m^g e^{i\gamma_m^g y} + b_m^g e^{-i\gamma_m^g y}\right), \tag{5c}$$

where $x_o^1 = 0$ and $x_o^2 = x_3$ are the x coordinates of the left vertical metal walls of grooves 1 and 2, respectively (see Fig. 1) and w_1 and w_2 are their respective widths. Additionally, for grooves with PEC sidewalls, μ_m and γ_m are as follows:

$$\mu_m^g = m\frac{\pi}{w_g}, \quad m = 0,1,\ldots, \tag{6}$$

$$\gamma_m^g = \left[\epsilon_g k_o^2 - \left(\mu_m^g\right)^2\right]^{1/2}. \tag{7}$$

Note that, throughout the remainder of this paper, the modes will be identified by their expansion coefficients I_n^t, R_n^t, I_n^b, R_n^b, a_m^1, b_m^1, a_m^2, and b_m^2. Also note that, because of the notation that has been chosen with the groove identifier in the superscript, the squares of the groove-2 quantities μ_m^2, γ_m^2, ϕ_m^2, and a_m^2 are denoted as $(\mu_m^2)^2$, $(\gamma_m^2)^2$, $(\phi_m^2)^2$, and $(a_m^2)^2$ to avoid confusion.

Two different calculations are performed in this paper. One calculation uses the full RCWA algorithm with only one incident beam, whose energy and angle of incidence are varied to obtain the reflectance and transmittance as a function of energy and incidence angle. From this reflectance curve, a PR dispersion curve is identified and is used as a comparison for the results obtained from the second calculation. The second calculation is the focus of this paper and involves the derivation and analysis of the PR dispersion relation.

III. RCWA AND ASYMMETRICAL EXCITATION

For the first calculation, all the symmetry of the system is destroyed by applying an incident beam only from the top of the structure and at off-normal angles of incidence. Thus, the full RCWA algorithm is needed for this problem in which there are no symmetry-enabled relations between the unknown field expansion coefficients R_n^t, R_n^b, a_m^1, b_m^1, a_m^2, and b_m^1.

Similar to what is performed in Ref. [6], boundary conditions (BCs) are imposed at the interfaces within the structure. Namely, continuity of H_z across the top entrance of groove 1 and groove 2, continuity of E_x over the entire unit cell at $y = h/2$, and three additional and similar BCs are imposed for the interfaces at $y = -h/2$. The resulting equations are cast into a matrix equation of the following form [6]:

$$M\Theta = \Psi, \tag{8}$$

where M is the coupling matrix, Θ is the column matrix of unknown field expansion coefficients, and Ψ is the column

matrix of initial conditions,

$$\Theta = (R \quad a^1 \quad b^1 \quad a^2 \quad b^2 \quad \widetilde{R})^\top, \tag{9a}$$

$$\Psi = \left(-AI \quad -BI \quad -\frac{\Lambda\beta}{\epsilon_s k_o} I \quad -A\widetilde{I} \quad -B\widetilde{I} \quad \frac{\Lambda\beta}{\epsilon_s k_o}\widetilde{I}\right)^\top, \tag{9b}$$

$$M = \begin{pmatrix} A & -N\phi^1 & -N(\phi^1)^{-1} & 0 & 0 & 0 \\ B & 0 & 0 & -N\phi^2 & -N(\phi^2)^{-1} & 0 \\ -\frac{\Lambda\beta}{\epsilon_s k_o} & \frac{C\gamma^1\phi^1}{\epsilon_1 k_o} & -\frac{C\gamma^1(\phi^1)^{-1}}{\epsilon_1 k_o} & \frac{D\gamma^2\phi^2}{\epsilon_2 k_o} & -\frac{D\gamma^2(\phi^2)^{-1}}{\epsilon_2 k_o} & 0 \\ 0 & -N(\phi^1)^{-1} & -N\phi^1 & 0 & 0 & A \\ 0 & 0 & 0 & -N(\phi^2)^{-1} & -N\phi^2 & B \\ 0 & \frac{C\gamma^1(\phi^1)^{-1}}{\epsilon_1 k_o} & -\frac{C\gamma^1\phi^1}{\epsilon_1 k_o} & \frac{D\gamma^2(\phi^2)^{-1}}{\epsilon_2 k_o} & -\frac{D\gamma^2\phi^2}{\epsilon_2 k_o} & \frac{\Lambda\beta}{\epsilon_s k_o} \end{pmatrix}, \tag{9c}$$

with R^t, I^t, a^1, b^1, R^b, I^b, a^2, and b^2 as column matrices of the field expansion coefficients, and the other matrix definitions are as follows:

$$A_{mn} = \sqrt{\frac{w_1}{2}}\left\{e^{i\mu_m^1 w_1/2}\mathrm{sinc}\left[\left(\alpha_n + \mu_m^1\right)\frac{w_1}{2}\right] + e^{-i\mu_m^1 w_1/2}\mathrm{sinc}\left[\left(\alpha_n - \mu_m^1\right)\frac{w_1}{2}\right]\right\}, \tag{10}$$

$$B_{mn} = e^{i\alpha_n(x_3 - w_1/2)}\sqrt{\frac{w_2}{2}} \times \left\{e^{i(\alpha_n + \mu_m^2)w_2/2}\mathrm{sinc}\left[\left(\alpha_n + \mu_m^2\right)\frac{w_2}{2}\right] + e^{i(\alpha_n - \mu_m^2)w_2/2}\mathrm{sinc}\left[\left(\alpha_n - \mu_m^2\right)\frac{w_2}{2}\right]\right\}, \tag{11}$$

$$N_{mp} = \begin{cases} 2, & \text{if} \quad m = p = 0, \\ 1, & \text{if} \quad m = p \neq 0, \\ 0, & \text{otherwise}, \end{cases} \tag{12}$$

$$\phi_{mp}^g = \begin{cases} e^{i\gamma_m^g h/2}, & \text{if} \quad m = p, \\ 0, & \text{if} \quad m \neq p, \end{cases} \tag{13}$$

with $C_{nm}(\alpha_n) = A_{mn}(-\alpha_n)$ and $D_{nm}(\alpha_n) = B_{mn}(-\alpha_n)$.

For the first calculation with only a single excitation beam, incident from the top of the structure, one has

$$I_n^t = \begin{cases} 1, & \text{if} \quad n = 0, \\ 0, & \text{if} \quad n \neq 0, \end{cases} \tag{14a}$$

$$I_n^b = 0 \quad \text{for all } n. \tag{14b}$$

The values of ω and k_x of this incident beam will be varied over all possible values below the onset of the far-field diffraction. Once this incidence condition is given, the full RCWA algorithm is used to solve for the reflectance $|R_0|^2$ and the transmittance $|\widetilde{R}_0|^2$.

Consider a lossless CTG shown in Fig. 1 that is composed of lossless materials, has a period of $\Lambda = 1.495$ μm, a film thickness of $h = 1.5$ μm, PEC as the metal, vacuum as the superstrate and substrate, and two vacuum-filled grooves per unit cell with groove 1 having a width of $w_1 = 0.25$ μm and with groove 2 having a width of $w_2 = 0.245$ μm with equal spacings between the grooves of $s_{12} = s_{21} = 0.5$ μm. Thus, the only difference between the grooves is the small 5-nm difference in widths, but this slight difference is enough to produce a PR that, at normal incidence ($k_x = 0$), occurs at $E_{pr} = 0.3375$ eV. Note that, for a lossless structure, *any* relative difference in the two grooves that breaks the mirror symmetry about Plane A (Fig. 1), regardless of how small, and will yield a structure that can support a PR [24]. The transmittance as a function of energy ($\hbar\omega$) and k_x is shown in Fig. 3. The optical properties of PRs have been described in Refs. [8,20,24], but one interesting thing to note at this point is that this PR band has a negative group velocity for all energies and momentum except for $k_x = 0$; this predicts that, when an incident beam has a momentum in the $+\hat{x}$ direction, the PR will have a flow of energy in the $-\hat{x}$ direction [24]. As stated before, the optical properties of the PRs in this structure are numerically modeled and are described in Refs. [8,20,24]; thus, let us move on to the main focus of this paper, namely, the derivation and analysis of the dispersion relation of PRs using the analytic model.

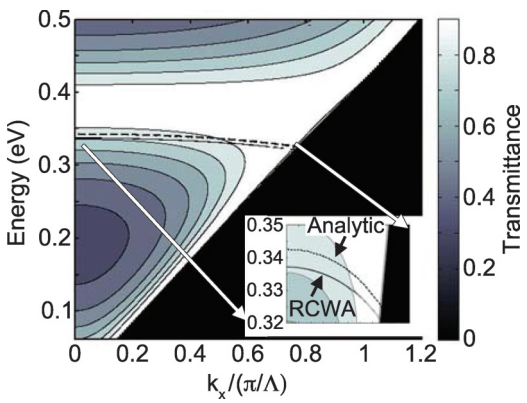

FIG. 3. (Color online) The transmittance of the 2-groove CTG with $\Lambda = 1.495$, $h = 1.5$, $w_1 = 0.25$, $w_2 = 0.245$ μm, $\epsilon_s = \epsilon_1 = \epsilon_2 = 1$, and equal wire widths $s_{12} = s_{21} = 0.5$ μm. There is a broad bandwidth transmission peak centered about 0.375 eV due to a WCM and a very narrow bandwidth PR band at 0.3375 eV for $k_x = 0$ and with a negative group velocity. The otherwise high transmission of the WCM is flipped by the PR to produce close-to-unity reflectance. The inset shows an expanded view of the PR dispersion curve, showing that the analytic equation provides a good approximation to the result obtained from the full RCWA.

IV. SYMMETRIC EXCITATION AND THE PHASE RESONANCE DISPERSION RELATION

Consider the situation where the structure is excited by beams incident from the top and bottom of the system. Due to the mirror symmetry of the physical structure about the x-z plane, if the incident beams have the same magnitude, k_x, and phase, then using Eqs. (8) and (9), it is easy to show that $R_m = \tilde{R}_m$, $a_m^1 = b_m^1$, and $a_m^2 = b_m^2$ and that Eqs. (8) and (9) reduce down to two identical smaller sets of equations. This smaller set of equations is expressed as

$$\hat{M}\hat{\Theta} = \hat{\Psi}, \tag{15}$$

where $\hat{M}$, $\hat{\Theta}$, and $\hat{\Phi}$ are now

$$\hat{\Theta} = (R \quad a^1 \quad a^2)^\top, \tag{16a}$$

$$\Psi = \left(-AI \quad -BI \quad -\tfrac{\Lambda\beta}{\epsilon_s k_o} I_0\right)^\top, \tag{16b}$$

$$\hat{M} = \begin{pmatrix} A & -N[\phi^1 + (\phi^1)^{-1}] & 0 \\ B & 0 & -N[\phi^2 + (\phi^2)^{-1}] \\ -\frac{\Lambda\beta}{\epsilon_s k_o} & \frac{C\gamma^1}{\epsilon_1 k_o}[\phi^1 - (\phi^1)^{-1}] & \frac{D\gamma^2}{\epsilon_2 k_o}[\phi^2 - (\phi^2)^{-1}] \end{pmatrix}. \tag{16c}$$

When modeling the type of structures studied in this paper, namely, 2-groove CTGs with the two grooves in the unit cell having only a slight relative difference, it is seen that only particular modes in the superstrate, cavities, and substrate contribute to the PR. For this structure, just slightly perturbed away from being a SLG, the first-order Floquet modes (i.e., $R_{\pm 1}$ and $\widetilde{R}_{\pm 1}$) and the zeroth-order WCMs (i.e., a_0^1, b_0^1, a_0^2, and b_0^2) primarily compose the PR, and these expansion coefficients are much larger than all other field expansion coefficients, including the incident beams that excite the PR (i.e., I_0 and $\widetilde{I}_0$) (Fig. 4). Thus, we can reduce the set of equations given by Eq. (15) to a much smaller set of equations when a PR occurs. And once we let the perturbations in geometry and composition of the second groove relative to the first groove go to zero, namely, having $\epsilon_2 \to \epsilon_1 = \epsilon_g$, $w_2 \to w_1 = w$, as well as having $x_3 \to \Lambda/2$, then $\gamma_0^2 \to \gamma_0^1 = \gamma_0$ and Eqs. (16) yield the relations,

$$a_0^2 = -e^{ik_x(\Lambda/2)} a_0^1, \tag{17}$$

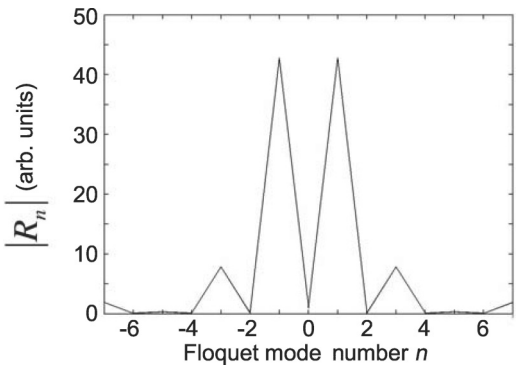

FIG. 4. The magnitudes of the Floquet modes (i.e., $|R_n|$) when the 0.3375-eV PR is excited. It is seen that, of the infinite number of possible Floquet modes, it is primarily the $R_{\pm 1}$ Floquet modes that compose the PR.

$$R_{-1} = \frac{2i\epsilon_s\gamma_0\sqrt{8w}}{\Lambda\epsilon_g\beta_{-1}} \mathrm{sinc}\left(\alpha_{-1}\frac{w}{2}\right) \sin\left(\gamma_0\frac{h}{2}\right) a_0^1, \tag{18}$$

$$R_1 = \frac{2i\epsilon_s\gamma_0\sqrt{8w}}{\Lambda\epsilon_g\beta_1} \mathrm{sinc}\left(\alpha_1\frac{w}{2}\right) \sin\left(\gamma_0\frac{h}{2}\right) a_0^1, \tag{19}$$

along with the equation that describes the dispersion of the PR,

$$\frac{2i\gamma_0}{\epsilon_g} \tan\left(\gamma_0\frac{h}{2}\right) = \frac{\beta_1\beta_{-1}(\Lambda/\epsilon_s w)}{\beta_1 \mathrm{sinc}^2\left(\alpha_{-1}\frac{w}{2}\right) + \beta_{-1}\mathrm{sinc}^2\left(\alpha_1\frac{w}{2}\right)}. \tag{20}$$

V. DISCUSSION

Equation (20) provides a description on the frequencies of PRs as a function of structural geometry, composition, and momentum. The values that Eq. (20) predict, along with the values obtained using the full RCWA algorithm, are shown in Fig. 3. It is seen that there is good agreement between the two methods, yet there are some slight differences between the values predicted by Eq. (20) and the RCWA values. However, the analytic model and Eq. (20) provide a way to quickly obtain a good approximation for the full dispersion curve of PRs that would otherwise require long computing times to generate by using FEM, FDTD, modal methods, or other methods. Once the approximate properties are obtained, these other methods can be used to obtain more accurate values for the frequencies of PRs.

To assess the accuracy of Eq. (20) and its range of applicability, 14 variations of the 2-groove CTG are modeled with the full RCWA, and the energies of the PRs are compared with the results obtained from Eq. (20). The aspect of the structure that is expected to most affect the accuracy of Eq. (20) is the width of the grooves relative to the total width of the unit cell, i.e., Λ. Thus, the 14 structures all have a period of $\Lambda = 1.495$ μm, a film thickness of $h = 1.5$ μm, with vacuum in the grooves, superstrate, and substrate; but the widths of the grooves and wires change such that the fractional area of the unit cell occupied by both grooves (f) varies from $f = 6\%$ to $f = 93\%$. Showing the full dispersion curves for all 14 structures is not necessary because they all show similar results, namely, a high degree of agreement between the full RCWA and Eq. (20), yet, particular situations are shown in Figs. 3 and 5–7. Figures 3, 5, and 6 show the complete PR dispersion curves for three structures with medium ($f = 66.5\%$), low ($f = 6.4\%$), and high ($f = 93.3\%$) values of f. Two angles of incident light are investigated further, namely, 0° (i.e., normal incidence) and light incident at a glancing angle to the structure, namely, $\sim 90^\circ$. In Fig. 7, it is seen that the accuracy of Eq. (20) in predicting the energies of PRs excited by $\sim 90^\circ$ incident light is comparable to the accuracy of Eq. (20) for normal incident light. Thus, in all 14 structures, for structures with narrow grooves and structures with wide grooves, for normal incident light and for glancing light, Eq. (20) predicts, to a high degree of accuracy, the values of energies of the PRs of particular momenta and accurately predicts the general shape of the dispersion curve.

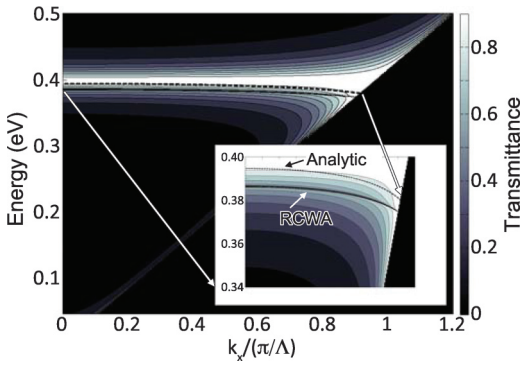

FIG. 5. (Color online) The transmittance of the 2-groove CTG with $\Lambda = 1.495$, $h = 1.5$, $w_1 = 0.05$, $w_2 = 0.0495$ μm, $\epsilon_s = \epsilon_1 = \epsilon_2 = 1$, and equal wire widths $s_{12} = s_{21} = 0.697\,75$ μm. The inset shows an expanded view of the PR dispersion curve, both the energies of the PRs and the shape of the dispersion curve are accurately predicted by Eq. (20) when compared to the results obtained from the full RCWA.

There is one important caveat to the proceeding discussion on the accuracy of Eq. (20) and an additional restriction on the use of the equation. Equation (20) assumes that there are no other electromagnetic modes with energies close to those of the PRs. If there are, then these modes can produce "anticrossing," pushing the dispersion curve of the PR up or down in the ω-k plot as is seen in many other photonic structures.

If the two exciting beams are of normal incidence such that $k_x = 0$, then (20) can be set into the form

$$\frac{4i\epsilon_s}{\pi\epsilon_g\beta_1}\gamma_0\tan(\gamma_0 h/2) = \frac{1}{\frac{\pi w}{\Lambda}\mathrm{sinc}^2(\pi w/\Lambda)}, \tag{21}$$

where β_1 and γ_0 are given by

$$\beta_1 = \sqrt{\epsilon_s\frac{\omega^2}{c^2} - \left(\frac{2\pi}{\Lambda}\right)^2} = i\sqrt{\left(\frac{2\pi}{\Lambda}\right)^2 - \epsilon_s\frac{\omega^2}{c^2}}, \tag{22}$$

$$\gamma_0 = \sqrt{\epsilon_g}\frac{\omega}{c}, \tag{23}$$

with the radicand in the right-most side of Eq. (22) being positive (i.e., $2\pi/\Lambda < \sqrt{\epsilon_s}\omega/c$).

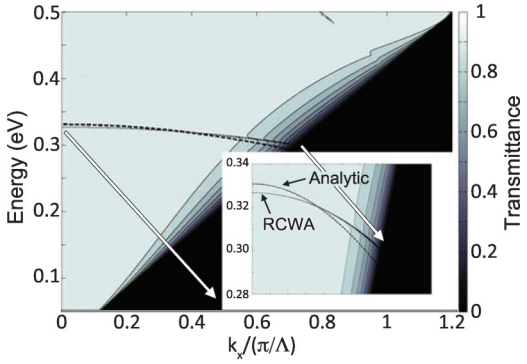

FIG. 6. (Color online) The transmittance of the 2-groove CTG with $\Lambda = 1.495$, $h = 1.5$, $w_1 = 0.7$, $w_2 = 0.695$ μm, $\epsilon_s = \epsilon_1 = \epsilon_2 = 1$, and equal wire widths $s_{12} = s_{21} = 0.05$ μm. The inset shows an expanded view of the PR dispersion curve using RCWA and Eq. (20).

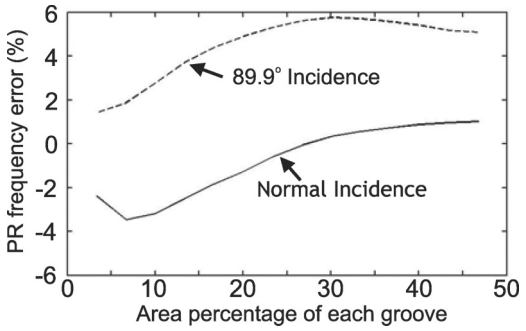

FIG. 7. The percent difference between the energies of the PRs computed using the full RCWA and the derived dispersion curve [Eq. (21)] for 14 structures with the same film thickness ($h = 1.5$ μm), period ($\Lambda = 1.495$ μm), and materials (vacuum and PEC) but with progressively larger groove widths and smaller wire widths and for angles of incidence of 0° and 89.9°. It is seen that the errors are small for normal incidence and wider groove widths but become larger for higher angles of incidence.

Concerning the task of designing a CTG with PR properties suitable for particular applications, it is useful to note that the left-hand side of Eq. (21) is dependent on many aspects of the structure, but most importantly, it is dependent on the frequency ω and *not* dependent on the width w, whereas, the right side is dependent on the width w but *not* on ω (Fig. 8). This provides an easy way to tune the wavelength of the PR by plotting the left side of the equation and then choosing the width necessary for Eq. (21) to be satisfied at the desired wavelength.

Another interesting aspect of Eq. (21) is what it predicts for the relationship between the wavelength of the transmission peak of the WCM and the wavelength of the PR (i.e., $\lambda_{pr} = 2\pi c/\omega_{pr}$). With the type of SLG and CTG studied in this paper with vacuum in the superstrate and substrate, the wavelength of normal incident light that excites the WCM is approximately equal to twice the optical height of the groove (i.e., $\lambda_{\mathrm{WCM}} = 2\sqrt{\epsilon_g}h$). As is seen in Fig. 3, the transmission peak of the

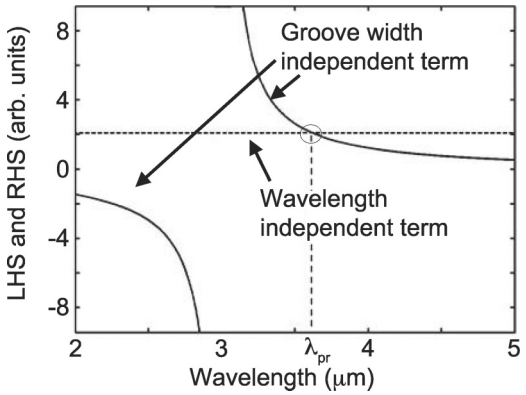

FIG. 8. The plot of the LHS and RHS of Eq. (21). The LHS is independent of groove width w, whereas, the RHS is independent of the wavelength or frequency. Thus, for a grating with a fixed period, thickness, and dielectric materials, the frequency of the PR $\omega_{pr} = 2\pi c/\lambda_{pr}$ can be tuned by adjusting the width of the groove while keeping constant all other parameters (e.g., period Λ, thickness h, and dielectric of the groove material ϵ_g).

WCM occurs at $\lambda = 3.25\ \mu$m (0.382 eV); the slightly higher wavelength of the WCM compared to $2\sqrt{\epsilon_g}h$ is attributed to the fact that the fields of this resonant mode are not entirely confined to the cavity but can extend out into the superstrate and substrate by a certain amount dependent on the Q of the WCM, making for a larger effective groove height than the actual geometric height [25]. Now, when looking at the LHS of Eq. (21), one sees that the tangent term produces a singularity at $\nu_0 h/2 = \pi/2$ (corresponding to the wavelength of normal incident light of $\lambda = 2\sqrt{\epsilon_g}h$) with the LHS diverging to $-\infty$ when approaching $\lambda = 2\sqrt{\epsilon_g}h$ from smaller values of λ and diverging to $+\infty$ when approaching $\lambda = 2\sqrt{\epsilon_g}h$ from larger values λ (Fig. 8). The RHS of Eq. (21), however, is independent of wavelength, always positive, and goes to infinity as $w \to 0$. Thus, the smallest wavelength for which the LHS and RHS intersect occurs when the RHS goes to infinity (when $w \to 0$) and occurs at $\lambda = 2\sqrt{\epsilon_g}h$. This value of $\lambda = 2\sqrt{\epsilon_g}h$ is then the *minimum wavelength that any PR can have* in a lossless CTG of height h and groove dielectric ϵ_g. The maximum value of λ_{pr} can be significantly larger than $2\sqrt{\epsilon_g}h$ as the groove widths are increased towards the maximum possible value of $\Lambda/2$.

For example, say that one wants to minimize λ_{pr} in a CTG by adjusting the groove width w while keeping the period Λ and all other aspects of the grating the same. Based on this analysis, one would minimize w. In doing so, the Q of the WCM would be increased (because it is proportional to h/w), and the transmission peak of the WCM would converge to $2\sqrt{\epsilon_g}h$, the same value that λ_{pr} is approaching. Thus, for a 2-groove CTG with two very narrow grooves with only a small dissimilarity, the PR will *bisect* the WCM transmission peak, yielding a narrow bandwidth transmission null within a larger bandwidth WCM-produced transmission peak as noted in Ref. [18].

It is clear that phase resonances are a type of Fano resonance (FR) with the three types of line shapes possible that are typical of FRs, including the asymmetric line shape typically associated with Fano resonances [26]. With FRs, one is interested in not only predicting the frequency of the resonance, but also predicting the line shape. A full discussion of the calculation of the bandwidths and line shapes of the FRs is outside the scope of this paper, but Ref. [26] details how the line shapes of the transmittance and reflectance can be calculated by using the detuning factor of the system, which itself is determined by the frequencies and bandwidths of the two slightly dissimilar and coupled cavities. Yet, one should exercise caution when attempting to use the line-shape equations described in Ref. [26] with the phase resonances described in this paper. This is because the individual cavity modes that compose the phase resonances can have very large bandwidths, and the equations in Ref. [26] would yield a small detuning factor, a small transmission, and a large reflectance when the FR (PR in this paper) is not excited. However, this is counter to what is observed with the phase resonances studied in this paper.

PRs can be used for high-finesse high-Q electromagnetic (EM) filters and for a new type of corrugated surface antenna (CSA). The Q of the PRs can be extraordinarily high (exceeding 10^6); as the relative differences of the grooves within the unit cell go to zero, the Q of the PRs goes to infinity for lossless structures [24]. With the ability to "dial in" the Q and frequencies of PRs [using Eq. (21)], EM filters can be designed that are only single-layer structures. Additionally, these filters can also serve as an antenna structure, similar to how CSAs are used and are configured [24]. CSAs that use PRs may provide benefits in terms of a wider range of properties, achievable through the appropriate design of the structure, as opposed to conventional CSAs that use TEM modes in the grooves.

Lastly, the aspect of competition between structural perturbation and loss and how it effects the dispersion curve is highly important for Fano resonances [27]. In an earlier paper of ours on the time-dependent excitation and decay of PRs, an analysis is performed on how loss affects PRs [24]. In Ref. [24], it is discussed that the more similar the two grooves are to each other (i.e., the smaller the perturbation), the stronger the enhanced EM fields of the PR and the narrower the bandwidth of the PRs are. It is then shown that, for particular structures with *real* metals (i.e., aluminum), PRs in the infrared spectral range ($\lambda = 8$–$12\ \mu$m) can exist and can cause a strong inversion in the transmissivity or opacity of the film, however, there is a certain amount of dissimilarity of the two grooves that is necessary to lower the enhancement of the EM fields associated with PRs such that the PR is not overdamped. In other words, if the two dissimilar grooves in the unit cell are not different enough, the PRs cannot be established because of prohibitively large optical losses in the metal wires. Yet, if the two grooves have a greater dissimilarity than this minimal necessary amount, the general trend is for decreasing absorption and increasing PR bandwidth for greater dissimilarity between the two grooves in the unit cell. The reader is referred to Ref. [24] for a more thorough discussion on the matter of loss and phase resonances.

VI. CONCLUSION

An analytic model was developed to describe the properties of phase resonances and to calculate their dispersion relation. It was found that these highly resonant light-concentrating modes are composed of particular electromagnetic modes in the grooves of the structure and in the layers above and below the structure. The dispersion relation of phase resonances was derived, providing a convenient tool to design compound transmission gratings that support phase resonances with particular properties, frequencies, and momenta. The analytical approach can be extended to calculate the dispersion relation for more-complicated compound grating structures that include more than two grooves in their unit cells. Applications of phase resonances include high-finesse electromagnetic filters and corrugated surface antennas that can be conformal to curved surfaces, light weight, and robust.

ACKNOWLEDGMENTS

This work was supported by the NSF Industry/University Cooperative Research Center for Metamaterials (Grant No. IIP-1068028) and by the AFOSR Bioenergy Project (Project No. FA9550-10-1-0350).

[1] T. W. Ebbesen, H. J. Lezec, H. F. Ghaemil, T. Thiol, and P. A. Wolff, Nature (London) **391**, 667 (1998).
[2] Z. Fan, L. Zhan, X. Hu, and Y. Xia, Opt. Commun. **281**, 5467 (2008).
[3] E. Popov, N. Bonod, M. Nevière, H. Rigneault, P.-F. Lenne, and P. Chaumet, Appl. Opt. **44**, 2332 (2005).
[4] H. Liu and P. Lalanne, Nature (London) **452**, 728 (2008).
[5] Q. Cao and P. Lalanne, Phys. Rev. Lett. **88**, 057403 (2002).
[6] D. Crouse, IEEE Trans. Electron Devices **52**, 2365 (2005).
[7] D. Crouse and P. Keshavareddy, Opt. Express **15**, 1415 (2007).
[8] D. Crouse, E. Jaquay, A. Maikal, and A. P. Hibbins, Phys. Rev. B **77**, 195437 (2008).
[9] W. Barnes, A. Dereux, and T. Ebbesen, Nature (London) **424**, 824 (2003).
[10] I. I. Smolyaninov, New J. Phys. **10**, 115033 (2008).
[11] M. Kadic, G. Dupont, S. Guenneau, and S. Enoch, in *Third International Workshop on Theoretical and Computational Nano-Photonics (TaCoNa-Photonics 2010)*, edited by D. R. Chigrin (AIP, New York, 2010) [AIP Conf. Proc. **1291**, 18 (2010)].
[12] Y. Liu, T. Zentgraf, G. Bartal, and X. Zhang, Nano Lett. **10**, 1991 (2010).
[13] M. Beruete, M. Navarro-Ćia, M. Sorolla, and D. C. Skigin, Opt. Express **18**, 23957 (2010).
[14] R. A. Depine, A. N. Fantino, S. I. Grosz, and D. C. Skigin, Optik (Stuttgart) **118**, 42 (2007).
[15] H. J. Rance, O. K. Hamilton, J. R. Sambles, and A. P. Hibbins, Appl. Phys. Lett. **95**, 041905 (2009).
[16] A. P. Hibbins, I. R. Hooper, M. J. Lockyear, and J. R. Sambles, Phys. Rev. Lett. **96**, 257402 (2006).
[17] M. Navarro-Cía, D. C. Skigin, M. Beruete, and M. Sorolla, Appl. Phys. Lett. **94**, 091107 (2009).
[18] D. Skigin and R. Depine, Phys. Rev. E **74**, 046606 (2006).
[19] D. C. Skigin and R. A. Depine, Opt. Commun. **262**, 270 (2006).
[20] A. Enemuo, M. Nolan, Y. Uk Jung, A. B. Golovin, and D. Crouse, J. Appl. Phys. **113**, 014907 (2013).
[21] A. N. Fantino, S. I. Grosz, and D. C. Skigin, Phys. Rev. E **64**, 016605 (2001).
[22] F. Medina, F. Mesa, and D. C. Skigin, IEEE Trans. Microwave Theory Tech. **58**, 105 (2010).
[23] D. C. Skigin, J. Opt. A, Pure Appl. Opt. **11**, 105102 (2009).
[24] I. Bendoym, A. B. Golovin, and D. T. Crouse, Opt. Express **20**, 22830 (2012).
[25] I. Mandel, E. Lansey, J. N. Gollub, and D. T. Crouse, Proc. SPIE **8457**, 845735 (2012).
[26] A. Miroshnichenko, S. Flach, and Y. Kivshar, Rev. Mod. Phys. **82**, 2257 (2010).
[27] A. Yakovlev and G. Hanson, IEEE Trans. Microwave Theory Tech. **48**, 67 (2000).